Editors' Suggestion

Less-ordered structures of silicene on Ag(111) surface revealed by atomic force microscopy

Jo Onoda,[1,*] Lingyu Feng,[2] Keisuke Yabuoshi,[2] and Yoshiaki Sugimoto[2]
[1]Department of Physics, University of Alberta, Edmonton, Alberta, Canada T6G 2J1
[2]Department of Advanced Materials Science, Graduate School of Frontier Sciences, The University of Tokyo, 5-1-5 Kashiwanoha, Kashiwa, Chiba 277-8561, Japan

(Received 8 August 2019; published 24 October 2019)

Silicene, a silicon analog of graphene, has the potential to become a candidate next-generation material by virtue of its novel physical and chemical properties. Although a rich variety of rotationally nonequivalent silicene structures have been observed with silicene grown on Ag(111) surfaces, the T phase, which has been considered a precursor phase, has a less-ordered structure, and thus, it is difficult to clarify its atomic structure. In this paper, we report the atomic structures of the T phase observed by high-resolution atomic force microscopy (AFM). While scanning tunneling microscopy images of the T phase show characteristic round dots, AFM reveals that the T phase has a continuous Si honeycomb arrangement, thus forming silicene. We identify two types of T phases with different silicene rotation angles with respect to the Ag substrate: the $(\sqrt{13} \times \sqrt{13})$ type-I T phase and the tiling-pattern T phase. The former has a unit cell corresponding to the conventionally proposed $(\sqrt{13} \times \sqrt{13})$ type I with less periodicity of Si buckling, while the latter is identified by the tessellation with four different rhombuses. We also investigate the T phase by site-specific force spectroscopy and find that some Si atoms at the T phase have slightly different chemical reactivities.

DOI: 10.1103/PhysRevMaterials.3.104002

I. INTRODUCTION

The discovery of graphene [1] has stimulated interest in exploring various new two-dimensional (2D) materials [2]. Among them, silicene has the potential to enable the ultimate miniaturization of Si devices for the semiconductor industry [3]. On the other hand, a recent surprising achievement in the field of 2D materials is that twisted bilayer graphene with a magic angle gives rise to exotic physical properties such as unconventional superconductivity [4] and the Mott insulating state [5]. These results naturally provoke the quest for the tunability of electronic properties in other atomically thin systems through interactions with supporting substrates. According to previous studies, silicene growth requires parent substrates such as Ag [6,7] and ZrB_2 [8]. As revealed by recent angle-resolved photoemission spectroscopy measurements [9,10], the electronic properties of silicene on Ag(111) can be modified by external periodic potentials originating from the interaction between the substrate and the overlayer. Thus, it is important to measure the rotation of the silicene sheet with respect to the substrate and the resulting buckling structure of Si atoms, which would induce novel electronic properties of silicene.

Silicene on Ag(111) surfaces has been intensively investigated as a prototypical system. A variety of superstructures have been observed, such as (4×4) [6,7,11–17], $(\sqrt{13} \times \sqrt{13})$R13.9° type II [7,11,13,18–26], and $(2\sqrt{3} \times 2\sqrt{3})$ [12–14,24,27–31] with respect to the Ag(111) unit cell. These phases are characterized by the rotation angle of the topmost silicene sheet with respect to the substrate. When we define α $(-30° < \alpha \leqslant 30°)$ as the rotation angle of silicene layer and set it as $\alpha = 0°$ in the (4×4) phase [25,30], $(\sqrt{13} \times \sqrt{13})$R13.9° type-II and $(2\sqrt{3} \times 2\sqrt{3})$ structures have $\alpha = 5.2°$ and 10.9°, respectively.

Among such various phases, the T phase emerges at the lowest-temperature regime where other ordered phases start to appear [32]. The T phase frequently coexists with (4×4) and $(\sqrt{13} \times \sqrt{13})$R13.9° type II but tends to disappear when annealed at relatively high temperature, leaving (4×4) and $(\sqrt{13} \times \sqrt{13})$R13.9° type-II phases on the Ag(111) surface. Thus, the T phase is considered a "precursor phase" for the other ordered phases. In scanning tunneling microscopy (STM) images, the T phase appears as big and round protrusions in a hexagonal arrangement [7,11,13,20,22,33] or parallel linear chains [34,35]. These less-ordered STM patterns make it difficult to investigate the detailed structure of the T phase, and several structural models have been proposed. This phase is initially interpreted as a partially disordered phase consisting of incomplete pieces of honeycomb Si rings [11,34,36]. On the other hand, it is suggested that the T phase is the (3.5×3.5)R26° phase originating from Si films but not forming silicene [33]. As for a silicene model for the T phase, the superstructure in a hexagonal arrangement is referred to as the $(\sqrt{13} \times \sqrt{13})R13.9°$ type-I phase [12,13,20,22]. The $(\sqrt{13} \times \sqrt{13})R13.9°$ type-I phase is supposed to have $\alpha = 27°$. While one of the suggested models has a unit cell where one Si atom distinctly protrudes upward and leads to the round dots in STM images [22,37,38], another model has a unit cell in which one Si hexagonal ring bumps up as a whole [12]. Hence, the structural model of the T phase is still under debate.

To overcome the limitations of STM imaging, we need structural analysis methods suitable for the T phase, whose domain is relatively small compared to other phases.

*jonoda@ualberta.ca

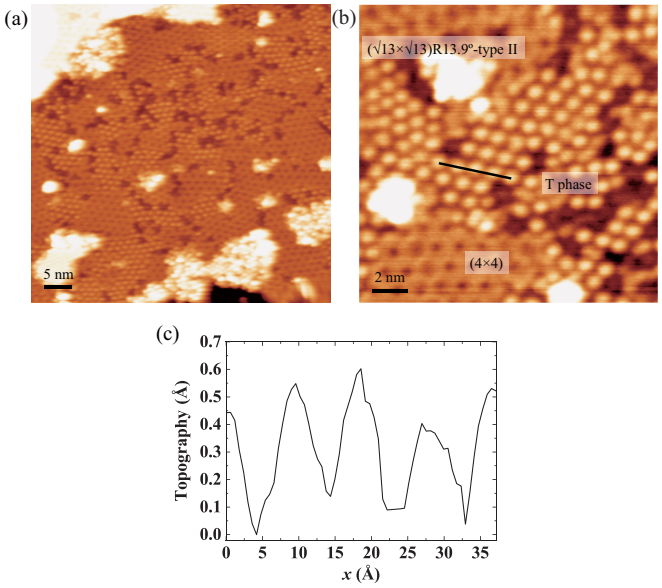

FIG. 1. (a) STM image of the mixture of the superstructures of silicene on Ag(111). Sample bias $V_S = -1.0$ V, tunneling current $I = 30$ pA. (b) STM image of the T phase. $V_S = -1.0$ V, $I = 30$ pA. (c) Line profile along the black line in (b).

Although diffraction methods such as low-energy electron diffraction [15] and grazing x-ray diffraction [38] are powerful tools for structural determination, these need a relatively large and uniformly formed area on the sample surface. On the other hand, atomic force microscopy (AFM) is a complementary method to STM. AFM can resolve all the constituent Si atoms of the (4×4) phase [17]. Subsequently, structural identification for the $(\sqrt{13} \times \sqrt{13})$R13.9° type-II phase is achieved by AFM [26]. In this paper, we report AFM observations of the T phase on the Ag(111) surface. We found that the complex structure of the T phase is composed of a continuous silicene sheet, and thus, the honeycomb structure made from Si atoms is retained. Depending on the rotation angle of α at the T phase, at least two types of short-range ordered superstructures were found; we refer to them as the $(\sqrt{13} \times \sqrt{13})$R13.9° type-I T phase and the tiling-pattern T phase, the latter of which is identified by the tessellation with four different rhombuses. We also conducted force spectroscopy at the T phase and the (4×4) phase and found that some Si atoms at the T phase have slightly different chemical reactivities than others.

II. EXPERIMENTAL METHODS

All experiments were carried out using a custom-built frequency-modulation AFM/STM at room temperature in ultrahigh vacuum (UHV; base pressure of 5×10^{-9} Pa). We used commercial Pt-coated or uncoated Si cantilevers, whose apices were cleaned by Ar^+ sputtering for removal of the native oxides. Our system is based on an optical fiber interferometer to detect the oscillation of mechanically excited cantilevers. When we carried out the AFM experiments, the voltage corresponding to the contact potential difference between the tip and sample was applied to the sample in order to minimize the effect of long-range electrostatic force. More details are described elsewhere [39]. Clean Ag(111) was prepared by repeated Ar^+ sputtering (2 keV, 1×10^{-3} Pa for 20 min) and annealing (600 °C) in UHV. The Si source for preparing silicene was achieved by resistively heating the Si wafer ($10 \times 3 \times 0.5$ mm^3). We deposited Si onto a clean Ag(111) surface by holding it at 230 °C.

III. RESULTS AND DISCUSSION

A. STM/AFM observations of the T phase

Figure 1(a) shows an STM image of the silicene prepared on the Ag(111) surface. About half of the total area in Fig. 1(a) represents well-ordered phases such as (4×4) and $(\sqrt{13} \times \sqrt{13})$R13.9° type II, while the other half shows round dots with a close-packed hexagonal arrangement. Except for these areas, the bright disordered islands on the terrace could be composed of expelled Ag atoms, which are formed during the initial growth [35]. Figure 1(b) shows a close-up of the dotted areas at the boundaries between the (4×4) and $(\sqrt{13} \times \sqrt{13})$R13.9° type-II phases. The line scan [Fig. 1(c)] as measured in Fig. 1(b) gives us an approximately 1-nm distance between nearest-neighbor protrusions. Thus, the area should correspond to the T phase observed in the previous STM studies [7,11,13,20,22,33].

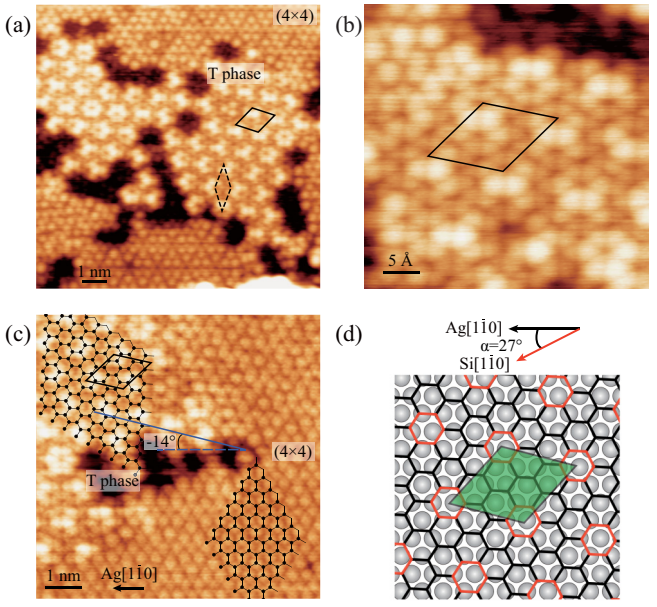

FIG. 2. (a)–(c) AFM images of the $(\sqrt{13} \times \sqrt{13})$ type-I T phase. Unit cells are represented by black rhombuses. (a) The dashed black rhombus represents an irregular unit cell. The acquisition parameters are the resonance frequency $f_0 = 136.056$ kHz, the cantilever-oscillation amplitude $A = 150$ Å, the spring constant $k = 21.9$ N/m, $V_S = 294$ mV, and $\Delta f = -12.3$ Hz. (b) $f_0 = 154.612$ kHz, $A = 150$ Å, $k = 26.2$ N/m, $V_S = -27$ mV, $\Delta f = -16.6$ Hz. (c) $f_0 = 133.146$ kHz, $A = 150$ Å, $k = 20.5$ N/m, $V_S = -145$ mV, $\Delta f = -21.8$ Hz. (d) Structural model for the $(\sqrt{13} \times \sqrt{13})$ type-I T phase. The black honeycomb lattice and balls represent silicene and Ag atoms, respectively. Red hexagonal rings in the silicene honeycomb lattice represent bumped hexagonal rings at the T phase in the AFM image. The green rhombus represents a unit cell.

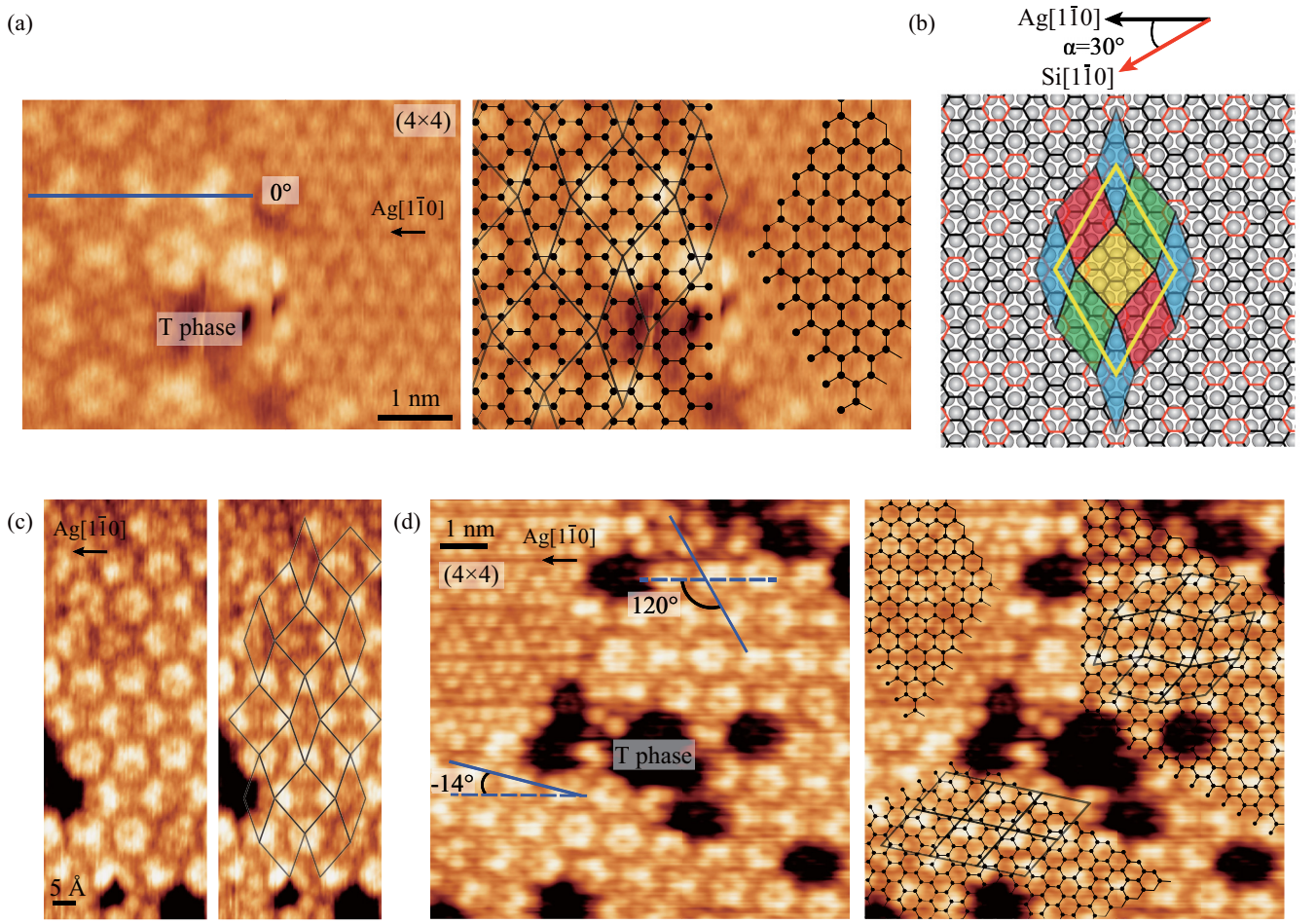

FIG. 3. (a), (c), and (d) AFM images of the tiling-pattern T phase. Unit cells are represented by four black rhombuses. (a) $f_0 =$ 153.407 kHz, $A = 168$ Å, $k = 28.4$ N/m, $V_S = 0$ mV, $\Delta f = -11.0$ Hz. (b) Structural model for the tiling-pattern T phase. The black honeycomb lattice and balls represent silicene and Ag atoms, respectively. Red hexagonal rings in the silicene honeycomb lattice represent bumped hexagonal rings at the T phase in the AFM image. Four rhombuses are colored red, green, yellow, and blue. The large yellow rhombus represents the unit cell corresponding to (7×7) with respect to Ag(111)-(1×1). (c) $f_0 = 153.407$ kHz, $A = 168$ Å, $k = 28.4$ N/m, $V_S =$ 0 mV, $\Delta f = -10.6$ Hz. (d) $f_0 = 136.056$ kHz, $A = 150$ Å, $k = 21.9$ N/m, $V_S = 122$ mV, $\Delta f = -18.3$ Hz.

We conducted AFM observations of such dotted areas in the topographic mode. As represented in Figs. 2(a)–2(c), AFM topographic images reveal the detailed atomic structures of the T phase. We found that the round dots observed in the STM images are hexagonal rings. As shown in Fig. 2(b), a continuous honeycomb pattern is clearly visualized at the T phase. Moreover, the same silicene honeycomb lattice can be superimposed at both the T phase and the (4×4) phase [Fig. 2(c)]. Thus, the T phase can be regarded as a continuous silicene sheet. This result rules out the previous interpretations that the T phase is an incomplete silicene lattice [11,36]. We can define the center of each bright hexagonal ring as the corner of the unit cell of the superstructure [Fig. 2(b)], although we found that the $(\sqrt{13} \times \sqrt{13})$ type-I T phase has some irregular unit cells, as represented by the dashed black rhombus in Fig. 2(a). The angle between Ag[1$\bar{1}$0] and the line where the bright honeycomb rings align with the nearest-neighbor distance [blue line in Fig. 2(c)] is estimated to be about $-14°$. We also measured the rotation angle of α at the T phase in Fig. 2(c), the result of which is 27°. Note that because of the mirror symmetry with respect to Ag[1$\bar{1}$0], we also found the T phase with $\alpha = -27°$ as well (not shown). The coexisting (4×4) also enables us to figure out the positions of underlying Ag atoms. On the basis of this result, we construct the structural model shown in Fig. 2(d) [here, we use lattice constants of $a_{\mathrm{Ag}} = 2.89$ Å for Ag(111)-(1×1) and $a_{\mathrm{silicene}} = 3.84$ Å for silicene-(1×1)]. The primary feature of the buckling pattern of silicene is the same as the one in Ref. [12] for $(\sqrt{13} \times \sqrt{13})$R13.9° type I, clearly ruling out another plausible structural model with one Si atom in a unit cell protruding upward [22,37,38]. We thus refer to this type of T phase as the $(\sqrt{13} \times \sqrt{13})$ type-I T phase. However, when we focus on the details of the brighter hexagonal rings in the unit cell [Figs. 2(a)–2(c)], we see a variation in the vertical positions of the Si atoms, and the pattern of the bumped Si atoms is less periodic. The features of the Si atoms in the hexagonal rings with different heights and less periodicity can explain the previous STM observation that there are two or three smaller protrusions with different rotations inside the big protrusions [11]. It should be noted that the ideal model for $(\sqrt{13} \times \sqrt{13})$R13.9° type I, where the Si atoms in the hexagonal rings are leveled, is found to be energetically

unfavorable in the theoretical calculations [38]. We speculate that the less-periodic deformation of the Si hexagonal rings could play some role in stabilizing the $(\sqrt{13} \times \sqrt{13})$ type-I T phase.

Figure 3(a) shows a different type of T phase from the $(\sqrt{13} \times \sqrt{13})$ type-I T phase. This kind of T phase has a characteristic in which the line where the bright honeycomb rings align with the nearest-neighbor distance [blue line in Fig. 3(a)] is directed toward Ag[$1\bar{1}0$]. By superimposing the silicene honeycomb lattice on the AFM image [Fig. 3(a)], α is estimated at 30°. By connecting the center of each bright hexagonal ring in Fig. 3(a), we found that the T phase can be expressed by the tessellation of four kinds of rhombuses. Considering the underlying Ag atoms, we can draw a model for this T phase, as shown in Fig. 3(b). The four kinds of rhombuses have the same lattice constant of $\sqrt{7}a_{\text{silicene}}$, two of which [red and green rhombuses in Fig. 3(b)] are similar to a unit cell of the $(\sqrt{13} \times \sqrt{13})R13.9°$ type-I T phase. We refer to this superstructure as the tiling-pattern T phase. In the tiling-pattern T phase, as highlighted in Fig. 3(b), we can find a large unit cell composed of the four kinds of rhombuses. The unit cell corresponds to the (7×7) phase with respect to Ag(111)-(1×1) or the $(3\sqrt{3} \times 3\sqrt{3})R30°$ phase with respect to silicene-(1×1), with 0.1% mismatch. We applied the above model to another T phase in Fig. 3(c). As a result, we found that the T phase can be characterized overall by the tessellation with the four different rhombuses, as represented in Fig. 3(c). The upward deformation of the bright honeycomb rings in the tiling-pattern T phase shows better regularity than the $(\sqrt{13} \times \sqrt{13})R13.9°$ type-I T phase; for example, in the rhombus in Fig. 3(c) which corresponds to the blue one in Fig. 3(b), the lower side of the tilted ring is toward the nearest ring among its neighboring rings. We guess such ordering might be related to the stability of the structure. We also observed the area where the $(\sqrt{13} \times \sqrt{13})$ type-I and tiling-pattern T phases are connected [Fig. 3(d)]. Comparing the tiling-pattern T phase in Fig. 3(d) with those in Figs. 3(a) and 3(c), we see that the pattern is rotated by 120° with respect to Ag[$1\bar{1}0$]. Considering the symmetry of Ag(111), the tiling-pattern T phase can have three different domains on the Ag surface. Even in a previous STM study [40], we can find some areas are characterized by the tiling-pattern T phase.

There are slight variations in the rotation angles of the T phase. We measured nine different T phases (not all images are shown) and obtained the range of rotation angle as $\alpha = \pm(27°–30°)$. Figures 4(a) and 4(b) show two examples of them, where α is estimated at $-28°$ and 29°, respectively. The difference between the rotation angles is subtle, but the resulting structures represent the $(\sqrt{13} \times \sqrt{13})$ type-I T phase and the tiling-pattern T phase, respectively. We found that some of the irregular unit cells in Fig. 4(a) are composed of some of the unit cells for the tiling-pattern T phase [yellow and blue rhombuses in Fig. 3(b)]. The variation of the rotation angle means that the T phase has relatively weak interactions with the Ag substrate compared to other well-ordered phases, such as the (4×4) and $(\sqrt{13} \times \sqrt{13})R13.9°$ type-II phases. Such flexibility of the rotation angle generally leads to incommensurate superstructures with respect to the substrate, eventually causing the less-ordered buckling pattern and thus less periodicity of the T phase.

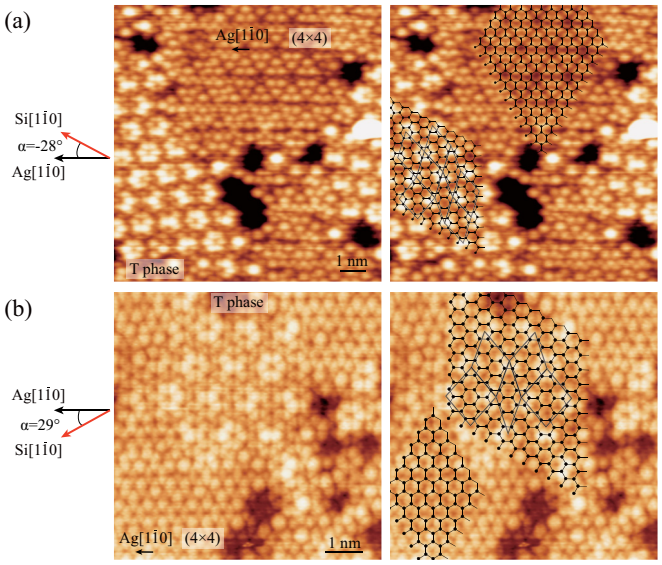

FIG. 4. (a) and (b) AFM images of the $(\sqrt{13} \times \sqrt{13})$ type-I T phase and tiling-pattern T phase, respectively. Unit cells are represented by black rhombuses. (a) $f_0 = 133.146$ kHz, $A = 150$ Å, $k = 20.5$ N/m, $V_S = -145$ mV, $\Delta f = -22.3$ Hz. (b) $f_0 = 136.056$ kHz, $A = 150$ Å, $k = 21.9$ N/m, $V_S = 0$ mV, $\Delta f = -28.3$ Hz.

B. Site-specific Force Spectroscopy

We investigated the chemical reactivities of surface atoms at the T phase. We performed force spectroscopy on higher and lower atoms at the T phase and also on an upper buckled Si atom at the (4×4) phase, which are referred to as the A, B, and C sites in Figs. 5(a) and 5(b), respectively. First, we measured the total frequency shift curves $\Delta f_{\text{Total}}(z)$ [Fig. 5(c)], which include components derived from both short-range (SR) and long-range (LR) forces. Then, we extracted $\Delta f_{\text{SR}}(z)$ curves by subtracting the $\Delta f_{\text{LR}}(z)$ curve from $\Delta f_{\text{Total}}(z)$, converting $\Delta f_{\text{SR}}(z)$ to $F_{\text{SR}}(z)$ [Fig. 5(d)] using the standard method [41]. By comparing the $F_{\text{SR}}(z)$ curves in Fig. 5(d), we see that the maximum attractive forces at the A, B, and C sites have values similar to each other within about 10%. Since the maximum attractive force represents the fingerprint of the chemical identity of a surface atom [42,43], this result corroborates further that the T phase is composed of Si atoms. However, when we look at the details, we see that the maximum attractive force at site A shows slightly higher chemical reactivity compared to the others [Fig. 5(d)]. This could be explained by the difference in the bond angles of surface atoms [44], indicating that the T phase is composed of differently buckling Si atoms. The different chemical reactivities of Si atoms at the T phase suggest the potential tunability of the electronic properties of silicene by selective adsorption of gaseous atoms to such reactive sites [45].

It is worth noting that the high-resolution imaging of the T phase is operated in a regime where almost the maximum attractive forces are exerted [Fig. 5(d)]. This result is consistent with previous ones regarding force spectroscopy on (4×4) [17] and $(\sqrt{13} \times \sqrt{13})R13.9°$ type II [26], indicating the pulling up of surface Si atoms by the AFM tip. We can call the high-resolution AFM imaging realized by the pulling up of surface atoms "active imaging" since surface atoms are

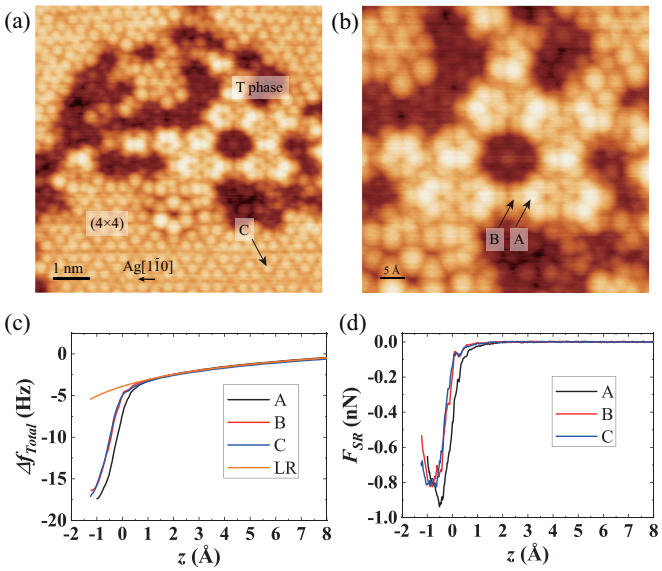

FIG. 5. (a) AFM images of the T phase and (4×4) phase. (b) Magnified image of the T phase in (a). $f_0 = 134.062\,\mathrm{kHz}$, $A = 150\,\text{Å}$, $k = 21.9\,\mathrm{N/m}$, $V_S = 294\,\mathrm{mV}$, $\Delta f = -10.3\,\mathrm{Hz}$. (c) $\Delta f_{\mathrm{Total}}$ curves measured on higher (A) and lower (B) atoms at the T phase and on the upper buckled Si atom (C) at the (4×4) phase. The background LR force is also represented. The origin ($z = 0$) corresponds to the topographic height when the tip is located above site A. (d) $F_{\mathrm{SR}}(z)$ curves on the A, B, and C sites.

actively perturbed by the AFM tip, in contrast to imaging by a CO-functionalized tip [46]. For stable active imaging in the topographic mode, a relatively large oscillation amplitude is needed. Otherwise, if we oscillate a tip at small amplitude (about 0.1 Å), we detect only SR forces. This would make it more difficult to perform a stable AFM operation because the sign of the slope of the $\Delta f_{\mathrm{Total}}(z)$ curve in such a force regime can change and the AFM topographic mode would thus be out of control. As shown in Fig. 5(c), the component from the LR forces is somewhat necessary to ensure the stable operation of the AFM topographic mode at a specific set point, promoting the active imaging of the silicene on the Ag(111) surface.

IV. SUMMARY

In summary, we observed the less-ordered T phase by high-resolution AFM and identified the round dots of the T phase observed by STM as hexagonal rings of silicene. Two different types of T phases were found: the $(\sqrt{13} \times \sqrt{13})$ type-I T phase with $\alpha = 27^\circ$ and the tiling-pattern T phase with $\alpha = 30^\circ$. The $(\sqrt{13} \times \sqrt{13})$ type-I T phase has a unit cell in which a Si hexagonal ring is protruded upward with less periodicity of Si buckling, while the tiling-pattern T phase is identified by the tessellation with four different rhombuses. The T phase has slight variations in the rotation angle α, indicating weak interactions with the Ag substrate. Site-specific force spectroscopy shows that some Si atoms at the T phase have slightly different chemical reactivities, which are presumably derived from the difference in the buckling of Si atoms. Our result obtained by active imaging in the AFM topographic mode settled the argument about the atomic structure of the T phase and can provide a route to investigate less-ordered or disordered structures in various 2D materials.

ACKNOWLEDGMENTS

We acknowledge the support from JSPS KAKENHI Grants No. JP18H03859 and No. 18K18990. Y.S. acknowledges the support of the Asahi Glass Foundation and Toray Science Foundation.

[1] K. S. Novoselov, A. K. Geim, S. V. Morozov, D. Jiang, M. I. Katsnelson, I. V. Grigorieva, S. V. Dubonos, and A. A. Firsov, Nature (London) **438**, 197 (2005).
[2] A. Molle, J. Goldberger, M. Houssa, Y. Xu, S.-C. Zhang, and D. Akinwande, Nat. Mater. **16**, 163 (2017).
[3] L. Tao, E. Cinquanta, D. Chiappe, C. Grazianetti, M. Fanciulli, M. Dubey, A. Molle, and D. Akinwande, Nat. Nanotechnol. **10**, 227 (2015).
[4] Y. Cao, V. Fatemi, S. Fang, K. Watanabe, T. Taniguchi, E. Kaxiras, and P. Jarillo-Herrero, Nature (London) **556**, 43 (2018).
[5] Y. Cao, V. Fatemi, A. Demir, S. Fang, S. L. Tomarken, J. Y. Luo, J. D. Sanchez-Yamagishi, K. Watanabe, T. Taniguchi, E. Kaxiras *et al.*, Nature (London) **556**, 80 (2018).
[6] P. Vogt, P. De Padova, C. Quaresima, J. Avila, E. Frantzeskakis, M. C. Asensio, A. Resta, B. Ealet, and G. Le Lay, Phys. Rev. Lett. **108**, 155501 (2012).
[7] C.-L. Lin, R. Arafune, K. Kawahara, N. Tsukahara, E. Minamitani, Y. Kim, N. Takagi, and M. Kawai, Appl. Phys. Exp. **5**, 045802 (2012).
[8] A. Fleurence, R. Friedlein, T. Ozaki, H. Kawai, Y. Wang, and Y. Yamada-Takamura, Phys. Rev. Lett. **108**, 245501 (2012).
[9] Y. Feng, D. Liu, B. Feng, X. Liu, L. Zhao, Z. Xie, Y. Liu, A. Liang, C. Hu, Y. Hu *et al.*, Proc. Natl. Acad. Sci. U.S.A. **113**, 14656 (2016).
[10] B. Feng, H. Zhou, Y. Feng, H. Liu, S. He, I. Matsuda, L. Chen, E. F. Schwier, K. Shimada, S. Meng, and K. Wu, Phys. Rev. Lett. **122**, 196801 (2019).
[11] B. Feng, Z. Ding, S. Meng, Y. Yao, X. He, P. Cheng, L. Chen, and K. Wu, Nano Lett. **12**, 3507 (2012).
[12] H. Jamgotchian, Y. Colignon, N. Hamzaoui, B. Ealet, J. Hoarau, B. Aufray, and J. Bibérian, J. Phys.: Condens. Matter **24**, 172001 (2012).
[13] D. Chiappe, C. Grazianetti, G. Tallarida, M. Fanciulli, and A. Molle, Adv. Mater. **24**, 5088 (2012).
[14] H. Enriquez, S. Vizzini, A. Kara, B. Lalmi, and H. Oughaddou, J. Phys.: Condens. Matter **24**, 314211 (2012).
[15] K. Kawahara, T. Shirasawa, R. Arafune, C.-L. Lin, T. Takahashi, M. Kawai, and N. Takagi, Surf. Sci. **623**, 25 (2014).

[16] A. Curcella, R. Bernard, Y. Borensztein, A. Resta, M. Lazzeri, and G. Prévot, Phys. Rev. B **94**, 165438 (2016).
[17] J. Onoda, K. Yabuoshi, H. Miyazaki, and Y. Sugimoto, Phys. Rev. B **96**, 241302(R) (2017).
[18] A. Resta, T. Leoni, C. Barth, A. Ranguis, C. Becker, T. Bruhn, P. Vogt, and G. Le Lay, Sci. Rep. **3**, 2399 (2013).
[19] Z. Majzik, M. R. Tchalala, M. Švec, P. Hapala, H. Enriquez, A. Kara, A. J. Mayne, G. Dujardin, P. Jelínek, and H. Oughaddou, J. Phys.: Condens. Matter **25**, 225301 (2013).
[20] Z.-L. Liu, M.-X. Wang, J.-P. Xu, J.-F. Ge, G. Le Lay, P. Vogt, D. Qian, C.-L. Gao, C. Liu, and J.-F. Jia, New J. Phys. **16**, 075006 (2014).
[21] C. Grazianetti, D. Chiappe, E. Cinquanta, G. Tallarida, M. Fanciulli, and A. Molle, Appl. Surf. Sci. **291**, 109 (2014).
[22] M. R. Tchalala, H. Enriquez, H. Yildirim, A. Kara, A. J. Mayne, G. Dujardin, M. A. Ali, and H. Oughaddou, Appl. Surf. Sci. **303**, 61 (2014).
[23] J. Zhuang, X. Xu, Y. Du, K. Wu, L. Chen, W. Hao, J. Wang, W. K. Yeoh, X. Wang, and S. X. Dou, Phys. Rev. B **91**, 161409(R) (2015).
[24] C. Grazianetti, D. Chiappe, E. Cinquanta, M. Fanciulli, and A. Molle, J. Phys.: Condens. Matter **27**, 255005 (2015).
[25] H. Jamgotchian, B. Ealet, H. Maradj, J. Hoarau, J. Bibérian, and B. Aufray, J. Phys.: Condens. Matter **28**, 195002 (2016).
[26] L. Feng, K. Yabuoshi, Y. Sugimoto, J. Onoda, M. Fukuda, and T. Ozaki, Phys. Rev. B **98**, 195311 (2018).
[27] J. Sone, T. Yamagami, Y. Aoki, K. Nakatsuji, and H. Hirayama, New J. Phys. **16**, 095004 (2014).
[28] E. Cinquanta, E. Scalise, D. Chiappe, C. Grazianetti, B. van den Broek, M. Houssa, M. Fanciulli, and A. Molle, J. Phys. Chem. C **117**, 16719 (2013).
[29] H. Enriquez, A. Kara, A. J. Mayne, G. Dujardin, H. Jamgotchian, B. Aufray, and H. Oughaddou, J. Phys.: Conf. Ser. **491**, 012004 (2014).
[30] H. Jamgotchian, B. Ealet, Y. Colignon, H. Maradj, J. Hoarau, J. Biberian, and B. Aufray, J. Phys.: Condens. Matter **27**, 395002 (2015).
[31] W. Wang, W. Olovsson, and R. I. G. Uhrberg, Phys. Rev. B **92**, 205427 (2015).
[32] R. Bernard, Y. Borensztein, H. Cruguel, M. Lazzeri, and G. Prévot, Phys. Rev. B **92**, 045415 (2015).
[33] R. Arafune, C.-L. Lin, K. Kawahara, N. Tsukahara, E. Minamitani, Y. Kim, N. Takagi, and M. Kawai, Surf. Sci. **608**, 297 (2013).
[34] K.-H. Wu, Chin. Phys. B **24**, 086802 (2015).
[35] M. R. Tchalala, H. Enriquez, A. J. Mayne, A. Kara, G. Dujardin, and H. Oughaddou, J. Phys.: Conf. Ser. **1081**, 012005 (2018).
[36] D. Kaltsas, L. Tsetseris, and A. Dimoulas, J. Phys.: Condens. Matter **24**, 442001 (2012).
[37] P. Pflugradt, L. Matthes, and F. Bechstedt, Phys. Rev. B **89**, 035403 (2014).
[38] A. Curcella, R. Bernard, Y. Borensztein, A. Resta, M. Lazzeri, and G. Prévot, Phys. Rev. B **99**, 205411 (2019).
[39] Y. Sugimoto, P. Pou, Ó. Custance, P. Jelinek, S. Morita, R. Pérez, and M. Abe, Phys. Rev. B **73**, 205329 (2006).
[40] J. Zhao, H. Liu, Z. Yu, R. Quhe, S. Zhou, Y. Wang, C. C. Liu, H. Zhong, N. Han, J. Lu *et al.*, Prog. Mater. Sci. **83**, 24 (2016).
[41] J. E. Sader and S. P. Jarvis, Appl. Phys. Lett. **84**, 1801 (2004).
[42] Y. Sugimoto, P. Pou, M. Abe, P. Jelinek, R. Pérez, S. Morita, and O. Custance, Nature (London) **446**, 64 (2007).
[43] J. Onoda, M. Ondráček, P. Jelínek, and Y. Sugimoto, Nat. Commun. **8**, 15155 (2017).
[44] N. Takagi, C.-L. Lin, K. Kawahara, E. Minamitani, N. Tsukahara, M. Kawai, and R. Arafune, Prog. Surf. Sci. **90**, 1 (2015).
[45] J.-w. Feng, Y.-j. Liu, H.-x. Wang, J.-x. Zhao, Q.-h. Cai, and X.-z. Wang, Comput. Mater. Sci. **87**, 218 (2014).
[46] L. Gross, F. Mohn, N. Moll, P. Liljeroth, and G. Meyer, Science **325**, 1110 (2009).